Publication P3

Alan Klanac, Sören Ehlers, and Jasmin Jelovica. 2009. Optimization of crashworthy marine structures. Marine Structures, volume 22, number 4, pages 670-690.

Marine Structures 22 (2009) 670–690

Contents lists available at ScienceDirect

Marine Structures

journal homepage: www.elsevier.com/locate/marstruc

Optimization of crashworthy marine structures

Alan Klanac*, Sören Ehlers, Jasmin Jelovica

Marine Technology Group, Department of Applied Mechanics, Helsinki University of Technology, P.O. Box 5300/Tietotie IC Espoo, 02015 TKK, Finland

ARTICLE INFO

Article history:
Received 22 September 2008
Received in revised form 27 April 2009
Accepted 16 June 2009

Keywords:
Crashworthiness
Optimization
Tanker
Safety
Structures

ABSTRACT

History shows that ferry and RoPax collisions with tankers can be devastating for human life. This paper follows up such a scenario to contribute to rational increase of safety of marine structures. Through the coupling of multi-objective structural optimization and crashworthiness analysis, a conventional tanker structure is optimized for higher collision tolerance, accounting for the change in hull mass, so that the increase in safety is efficient. Two new concepts, proposed here, are deemed necessary for the successful execution of this task: a 'two-stage' optimization approach, reducing the number of needed collision simulations, and a rapid collision simulation approach that utilizes coarse FE mesh and reduces calculation time. Combining the obtained results with the state-of-the-art knowledge, a new insight about crashworthy design of tanker structures is also realized.

1. Introduction

In 1991, in front of the Italian port of Livorno, ferry 'Moby Prince' struck into the anchored tanker 'Agip Abruzzo'. Oil on board the tanker burst out of the breached tank and caught fire that spread also to the ferry, killing in the end 140 people [1].

Many efforts have been spared lately to minimize the chance of such events. Yet, by looking into the data of IMO [2–6] following the dreaded incident, we can see that collisions consistently continue to plague on an annual basis some 20% of all serious and very serious marine accidents. 'Agip Abruzzo' was a single-hulled VLCC, but the nowadays double-hull ship structures still do not prevent the loss of hull integrity in the cases of collision with a large ferry such as 'Moby Prince'; see e.g. Ref. [7].

* Corresponding author. Tel.: +385 51 218 430x222; fax: +385 51 218 270.
E-mail addresses: alan.klanac@as2con.com, alan.klanac@tkk.fi (A. Klanac).

0951-8339/$ – see front matter © 2009 Elsevier Ltd. All rights reserved.
doi:10.1016/j.marstruc.2009.06.002

The concepts to make ships crashworthy, by redesigning their structure to maintain the hull integrity, have of late spurred a wide research interest. Generally, crashworthiness indicates a 'better' capability of some system to tolerate impact loads, and for ship-to-ship collisions, crashworthiness refers to an increased capacity of the struck ship to absorb kinetic energy prior to hull breach. Scientific study of crashworthiness of ships, however, has it roots in the past century, when Minorsky [8] showed that the deformed volume of hull structure relates proportionally with its crashworthiness. Unfortunately, this fact mislead many practitioners in concluding that improved crashworthiness would result in significant added mass of structure and thus in a reduction of ship's commercial competitiveness. Mostly for this reason, crashworthiness has not been adopted in commercial ship design, nor has it been widely indicated as a safety criterion. Furthermore, some newer studies [9,10] indicated that the increase in structural mass is not a sufficient, nor always a necessary condition for the increase of crashworthiness, and that crashworthiness can be increased with only a minor increase in mass if proper structural design is accomplished; see also Refs. [11,12].

Motivated by this situation, we aim here to deepen the knowledge on relations between hull crashworthiness and mass for practical marine structures. In particular, to concurrently optimize crashworthiness and mass of hull structure, and to obtain design alternatives that have maximal crashworthiness for a given hull mass. Since evaluation of crashworthiness is numerically challenging and time-consuming, we introduce in a new optimization approach. The approach fosters 'two-stage optimization' that reduces the overall computational effort needed to obtain the desired alternatives.

In Chapter 4, we illustrate this 'new optimization' with a practical example. Crashworthiness and a hull mass of a tanker are optimized, considering in addition the standard service load requirements. The optimization is performed for a critical accidental scenario resembling that of the 'Moby Prince' incident arguing that it can well represent the serious and very serious collisions. Furthermore, a special approach is applied to assess the crashworthiness rapidly and accurately, and with sensitivity to changes in structural scantlings.

2. Theoretical background

2.1. Practical optimization of marine structures

A structural optimization problem can be mathematically formalized with the following general formulation for constrained optimization

$$\min_{x \in \boldsymbol{X}} \left\{ \boldsymbol{f}(\boldsymbol{x}) | \boldsymbol{g}_j(\boldsymbol{x}) \geq 0, j \in [1, l] \cap \mathbb{Z}, m \geq 1 \cap \mathbb{Z} \right\}, \tag{1}$$

in which we search for a vector of variables $\boldsymbol{x} = (x_1, \ldots, x_n)^T$ that minimizes[1] the vector of design objectives $\boldsymbol{f}(x) = [f_1(\boldsymbol{x}), \ldots, f_m(\boldsymbol{x})]^T$, as well as satisfying the design constraints $\boldsymbol{g}(\boldsymbol{x}) = [g_1(\boldsymbol{x}), \ldots, g_l(\boldsymbol{x})^T]$. Alternatives satisfying the constraints are called feasible alternatives and are members of the feasible set $\boldsymbol{\Omega}$

$$\boldsymbol{\Omega} = \{ \boldsymbol{x} \in \mathbf{X} | \boldsymbol{g}(\boldsymbol{x}) \geq 0 \}, \tag{2}$$

where $\mathbf{X}$ is the set of all permutations $\mathbb{P}$ of design variable values x_i, between their lower $x_{\min}$ and upper $x_{\max}$ bounds of the variables, i.e. it contains all possible design alternatives,

$$\mathbf{X} = \left\{ \mathbb{P}(x_1, \ldots, x_n)^T | x_{\min} \leq x \leq x_{\max} \right\}. \tag{3}$$

The solution of optimization problem of Eq. (1) is a Pareto optimal alternative $\boldsymbol{x}^*$ which is non-dominated by other feasible alternatives, i.e. there is no feasible alternative better than $\boldsymbol{x}^*$ for all objectives. Such alternative is then rational and it belongs to a set of feasible Pareto optima $\hat{\boldsymbol{\Omega}}$, called

[1] It is well known that minimization of some objective can be linearly transformed into maximization, so the applicability of the presented theory onto maximization is assumed.

also the Pareto frontier. The Pareto frontier is then in general a subset to a set $\widehat{\mathbf{X}}$ of non-dominated design alternatives, $\widehat{\mathbf{\Omega}} \subseteq \widehat{\mathbf{X}}$. Thus,

$$\widehat{\mathbf{\Omega}} = \left\{ \boldsymbol{x}^* \in \mathbf{\Omega} \middle| \nexists \boldsymbol{x}^k, f_j\left(\boldsymbol{x}^k\right) < f_j(\boldsymbol{x}), \forall j \in [1,m], \forall \boldsymbol{x}^k \in \mathbf{\Omega} \setminus \boldsymbol{x}^* \right\}, \tag{4}$$

where

$$\widehat{\mathbf{X}} = \left\{ \boldsymbol{x} \in \mathbf{X} \middle| \nexists \boldsymbol{x}^k, f_j\left(\boldsymbol{x}^k\right) < f_j(\boldsymbol{x}), \forall j \in [1,m], \forall \boldsymbol{x}^k \in \mathbf{X} \setminus \boldsymbol{x} \right\}. \tag{5}$$

Practical optimization of ship structures ranges over hundreds of design variables, which are regularly treated as discrete. The number of design criteria, i.e. the constraints and objectives, is even larger. Furthermore, they are often evaluated through numerical calculations, as is also the case with crashworthiness. Fundamental optimization methods, e.g. those based on calculations of criteria gradients, cannot treat these problems successfully due to the unpredictable cavities arising in the design space related to large number of variables and non-linear criteria [13:588]. Some more complex approaches, e.g. decomposition of the global optimization problem into smaller manageable problems based on structural elements [14], or special sequential 'convex linearization' of the overall design space [15], are capable of handling practical problems, but they require explicit criteria knowledge. Following on the rise in computing power, *Genetic Algorithms* (GAs) [16–18] have lately become a convenient option for practical optimization problems. They deal directly and solely with the first order information about variable and criteria values and they can be programmed with ease to treat discrete variables. Due to the multi-point search and in-built randomness, they are capable of treating practical problems with large number of discrete variables and implicit criteria. But due to the same reasons, the experience shows that GAs demand significant amount of criteria evaluations. When coupled with FEM-based collision simulations, this presents an obstacle to optimize ship structure for crashworthiness in an acceptable time period.

In Refs. [19,20], a strategy characterized by 'vectorization' of the optimization problem is proposed to handle this problem. The constraint functions are transformed into additional objectives to be minimized alongside those original. This enables a focused search of the boundaries of the feasible domain where the optimal results are expected. Once implemented into a GA, vectorization permits a flexible optimization process, or the *omni-optimization*[2], so that e.g. one can use the same algorithm for both single- and multi-objective problems [22], or, as introduced with this paper, split the optimization into two stages. As we will show, this can save computational time which is a major benefit when optimizing crashworthiness.

2.2. Crashworthiness of marine structures

Ever since Minorsky's work [8], ship collisions have been studied as the decoupled manifestations of external dynamics of ship motions and internal mechanics of structural deformations. Former relates strongly to the momentum conservation of striking and struck ships, while latter depends strictly on their structural arrangements. Here, the focus is on structural design, so to evaluate the crashworthiness as specified above, we focus on the internal mechanics and assume independence between the changes in structural design and external dynamics. Internal mechanics of ship structures is typically simulated utilizing the non-linear 3D *Finite Element Method* (FEM). These simulations are time consuming, thus their application is regularly decoupled from dimensioning. They are mostly used for the final evaluation and analysis/approval; see e.g. Refs. [23–28]. Efforts have been spared however to reduce the computational time needed for internal mechanics [29–33]. But these approaches are not suitable for optimization where structure is persistently changed, as the adopted simplifications are established on a case-to-case basis.

[2] Deb and Tiwari [21] are credited for the term 'omni-optimization' to describe the procedure how a single algorithm (in this case 'omni-optimizer') can be applied both for single- and multi-objective optimization.

Up to now, optimization has been coupled with non-linear FEM-based collision simulations to increase crashworthiness in several studies, but mostly involving simple structures, or structural elements, where simulation time could be kept low. Notable examples involve topology optimization in two dimensions [34–36] and scantlings optimization in three dimensions (3D) utilizing meta-modelling, i.e. *Response Surface Method* (RSM) [37]. However, a possibility to extend these studies to the optimization of a complex, 3D ship hull structure is practically non-existent, reasons relating to a high number of involved design variables that demand extensive number of simulations. Therefore, the non-linear 3D FEM approach applied in this paper becomes essential to conduct optimization successfully.

3. A 'two-stage' optimization procedure

To optimize crashworthy marine structures, we propose to conduct it in two-stages. In the first stage the hull mass is optimized without calculating crashworthiness, and once the satisfactory reduction in mass is obtained, crashworthiness, as a computationally extremely expensive objective, is added to the optimization. The reason for proposing this approach follows the understanding of the problem at hand. On one hand, there are numerical complexities in minimization of structural mass, leading from the large number of design variables and non-linear criteria. On the other hand, we face timely crashworthiness calculations. Former demands generation and assessment of thousands of alternatives and latter, extends this very assessment to a great extent, necessitating weeks of computational time. Concurrent optimization of both of these objectives is therefore excessively time consuming, so utilizing the two-stage approach should help in reducing this time to a minimum.

Deb and Srinivasan [38] indicate that Pareto optimal alternatives of one system possess many commonalities. If this is valid for our problem, low crashworthy alternatives with low hull mass would share most of the variable values with crashworthy alternatives. Splitting therefore, the overall optimization problem as proposed should not significantly affect on the generation of rational alternatives. Minimization of hull mass independent of crashworthiness will provide thus the initial set of Pareto optimal alternatives in a significantly reduced optimization time. Starting to maximize crashworthiness from this set should in the end generate the complete set of Pareto optima.

3.1. Vectorization

Proposed approach to optimize crashworthy marine structures in two stages is based on vectorization [19,20]. The original problem of Eq. (1) is thus re-written to the following vectorized form:

$$\min_{\boldsymbol{x}\in\mathbf{X}}\left\{f_1(\boldsymbol{x}),\ldots,f_m(\boldsymbol{x}),f_{m+1}(\boldsymbol{x}),\ldots,f_{m+j}(\boldsymbol{x}),\ldots,f_{m+l}(\boldsymbol{x})\right\}, \tag{6}$$

The constraints $\boldsymbol{g}_j(\boldsymbol{x})$ are converted now into additional objectives $\{f_{m+1}(\boldsymbol{x}), \ldots, f_{m+j}(\boldsymbol{x})\}$ applying the unit-step representation [51]

$$f_{m+j}(\boldsymbol{x}) = \begin{cases} -g_j(\boldsymbol{x}), if\ \ g_j(\boldsymbol{x}) < 0 \\ 0, \qquad\quad otherwise \end{cases}, \forall j \in [1,l]. \tag{7}$$

The original optimization problem is now relaxed and also fully represented in the extended objective space $\mathbf{Y} = \{f_1(\boldsymbol{x}), \ldots, f_{m+l}(\boldsymbol{x}) | \boldsymbol{x} \in \mathbf{X}\}$. Applying the unit-step constraint transformation, all the feasible alternatives are strictly separated in the objective space from those that are infeasible. This makes the relative location of the Pareto frontier between the original objectives known. Fig. 1 illustrates this for the problem with a single original objective $f_1(\boldsymbol{x})$. We can see now that the feasible alternatives are strictly placed on the axis of the original objective. For the multi-objective problems, as studied here, the feasible alternatives are spread in the hyper-plane $\widehat{\mathbf{Y}}^{\boldsymbol{\Omega}} = \{f_1(\boldsymbol{x}), \ldots, f_m(\boldsymbol{x}) | \boldsymbol{x} \in \boldsymbol{\Omega}\}$ that contains then the Pareto frontier between the original objectives.

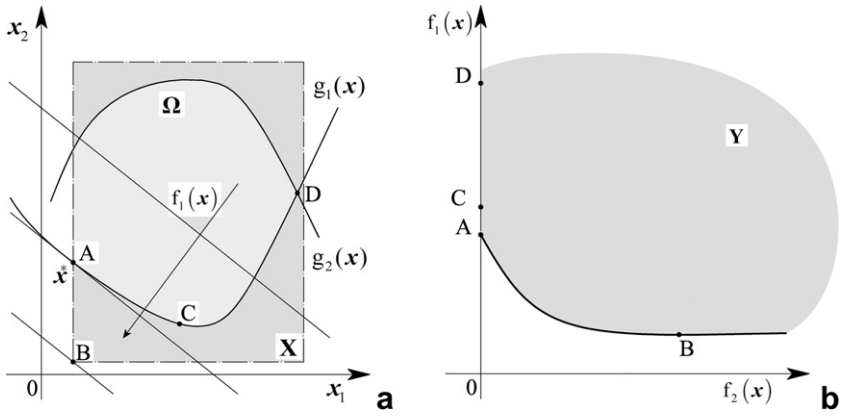

Fig. 1. Effect of unit-step constraint transformation on the characteristic alternatives (A – the feasible objective minimum, B – the infeasible objective minimum, C and D – feasible alternatives on the boundary) depicted in a) design space and b) objective space, where the objective $f_2(\boldsymbol{x})$ represents the constraint $g_1(\boldsymbol{x})$ after transformation using the Eq. (7). $\tilde{\mathbf{Y}}$ depicts the Pareto frontier between the original and the vectorized objectives, i.e. constraints.

3.2. VOP – a GA to perform optimization in two-stages

To solve the vectorized optimization problem and perform optimization in two stages, we employ a specific, binary-coded GA, VOP [19,20,22]; see Fig. 2. VOP's GA operators are standard [17], except the fitness function. The fitness of a design alternative $\boldsymbol{x}$ in generation i, $\varphi(\boldsymbol{x},i)$, is calculated as a function of the weighted Euclidean distance $d(\boldsymbol{x},i)$ that the alternative's normalized objective values $\bar{f}_j(\boldsymbol{x},i)$ close with the origin of the objective space $\mathbf{Y}$

$$\varphi(\boldsymbol{x},i) = \left(\max_{\boldsymbol{x}\in\mathbf{X}^i}[d(\boldsymbol{x},i)] - d(\boldsymbol{x},i)\right)^{\bar{d}(\boldsymbol{x},i)}. \tag{8}$$

where $\mathbf{X}^i$ marks the set, or population of alternatives at generation i. The weighted Euclidean distance is written as

$$\begin{aligned} d(\boldsymbol{x},i) &= \left\{\sum_j \left[w_j \bar{f}_j(\boldsymbol{x},i)\right]^2\right\}^{1/2}, \\ s.t. \quad & 0 \le w_j \le 1, \\ & \sum_j w_j = 1, \quad \forall j \in [1, m+l] \end{aligned} \tag{9}$$

Both the normalization of alternative's objectives $\bar{f}_j(\boldsymbol{x},i) = \alpha[f_j(\boldsymbol{x}),i]$, and of Euclidean distance[3] $\bar{d}(\boldsymbol{x},i) = \alpha[d(\boldsymbol{x},i)]$, is performed linearly. Hence, the applied normalization function[4] α for some function h at generation i is defined as

$$\alpha[h,i] = \frac{h - \max\limits_{\forall \boldsymbol{x}\in\mathbf{X}^i} h}{\max\limits_{\forall \boldsymbol{x}\in\mathbf{X}^i} h - \min\limits_{\forall \boldsymbol{x}\in\mathbf{X}^i} h}. \tag{10}$$

The weighting factors w_j of Eq. (9) determine the area of search focus in the objective space $\mathbf{Y}$. By

[3] In case that all design alternatives within a generation i are infeasible, the normalized 'distance' exponent $\bar{d}(\boldsymbol{x},i)$ of Eq. (8) disregards the value of original objectives and thus forces generation of feasible alternatives.

[4] If an objective is to be maximized, the numerator in Eq. (10) should change into $\min\limits_{\forall \boldsymbol{x}\in\mathbf{X}^i} \mathrm{h} - \mathrm{h}$.

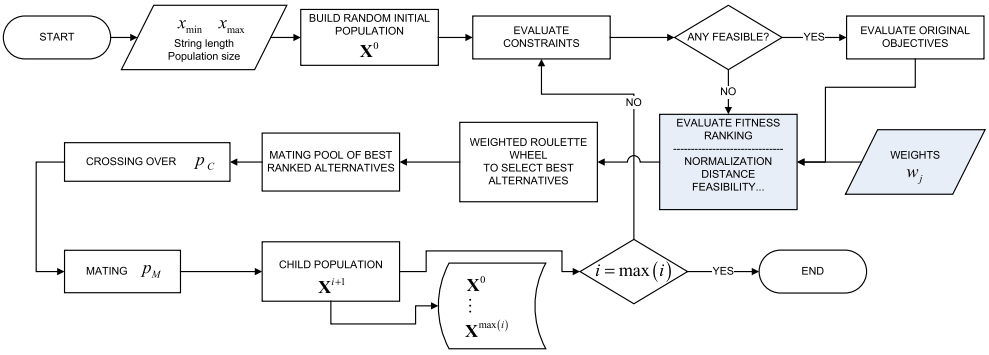

Fig. 2. Flow chart of VOP algorithm as applied in this paper, with specific genetic operators coloured in grey.

changing their values, one can decide whether to minimize more the constraint deviations or the original objectives, or some particular objective as seen in Fig. 3.

Obviously, it is easy to foresee that this very feature enables VOP to conduct the proposed optimization in two stages. The weighting factors change from the first to the second stage, changing the focus from hull mass minimization, needed to reach the initial set of the Pareto frontier, onto crashworthiness maximization, building the entirety of the frontier. Following Fig. 3, to attain Pareto optima, original objectives' weight factors $w_j, \forall_j \in [1,m]$ in Eq. (9) should possess low values as this combines strong minimization of the distance of designs to the boundaries of the feasible domain where minima

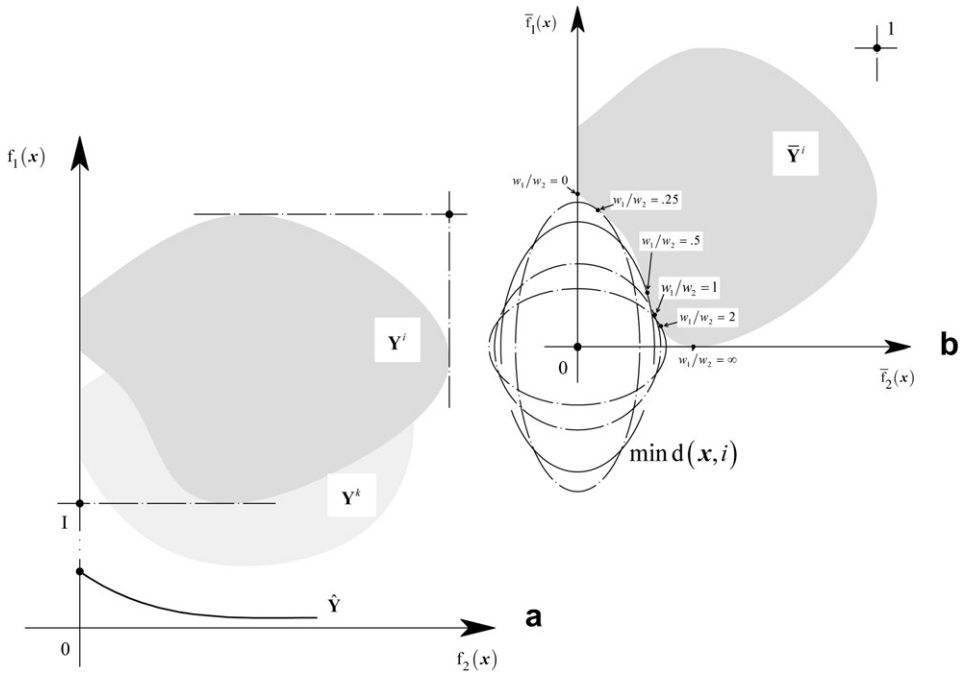

Fig. 3. 'Cloud' of design alternatives of generation $\mathbf{X}^i$ in the a) objectives space $\mathbf{Y}^i$ and b) after normalization $\mathbf{Y}^i$ according to Eq. (10). The normalized space (b) depicts the fitness determination for the generation *i*, specifically indicating the design alternative (•) having the minimal distance $d(\boldsymbol{x},i)$ to the point $\boldsymbol{I}$ with respect to the chosen weighting factors *w*. $\mathbf{Y}^k$ symbolizes the 'cloud' of design alternatives for some other generation *k*.

of the original objectives are usually found [20,22]. Furthermore, the original objectives' weight factors will not necessarily be the same. The objective that is more preferred should possess larger weight factor than the one less preferred. For the constraints-turned-objectives, the weight factors could be, for convenience, kept all equal. The following rule simplifies this argumentation:

$$0 \approx w_p \leq w_q \leq w_r, \quad p, q \in [1, m]; r \in [m+1, m+l] \tag{11}$$

where the minimization of the objective p is less preferred than that of the objective q, and r marks constraint(s). In the end, the actual values of weighting factors are determined heuristically, but as they bear physical meaning, they can be intuitively manipulated, as shown also in the next chapter.

4. Example: optimization of a crashworthy tanker structure

We illustrate now the 'two-stage' optimization of crashworthy marine structures on a realistic example. The aim is to improve the tanker structure's crashworthiness with the least added hull mass and with a capacity to sustain normal service loads.

4.1. Problem definition

Tanker is 180 m long, 32 m wide and 18 m deep, with a draught of 11.5 m. It has a typical product/chemical carrier construction as seen in Fig. 4, where the tanks are plated with stainless steel – *Duplex*. The collision is assumed to occur in the side shell of the cargo area amid two transverse bulkheads and at the draught of approx. 4 m, as seen in Fig. 5. Even though many probable collision scenarios are possible [39–41], we study here the tanker's crashworthiness in a 90° collision with roughly a 30 000 GRT RoPax or ferry, having an approximate draught of 7 m and a sufficient kinetic energy to cause rupture of the tanker's inner hull. This critical scenario is chosen for the extreme severity of its consequences and for its realistic chance of occurrence, e.g. in the Bay of Finland, Danish, or Dover straits, etc. where tanker and RoPax/ferry traffic intersect intensively. It is assumed therefore that this representative scenario can adequately indicate ship's crashworthiness, particularly to demonstrate the methodology presented in this paper.

4.1.1. Design objectives

Three objectives are considered for optimization: a) maximize the crashworthiness, i.e. hull capacity to absorb collision energy before being breached (abbreviated onwards as ENERGY), b) minimize the hull mass (abbreviated as HULL) and c) minimize the mass of stainless steel *Duplex* (abbreviated as DUPLEX). The maximization of ENERGY should increase ship safety, while the minimization of HULL and DUPLEX assures ship's commercial competitiveness. Particularly due to the costs, the mass of ship's hull is observed based on the material type. *Duplex* steel costs in the scale of ten times the standard high tensile steel including both material and labour costs. HULL and DUPLEX objectives are considered through the cross sectional area of the main frame multiplied by the length of the ship and steel density of 8000 kg/m^3. Evaluation of ENERGY is described in details in a chapter to follow.

4.1.2. Design variables

Tanker's longitudinally stiffened cargo space structure is split with transverse bulkheads placed every 17.8 m. The cargo tanks' plating is assumed to be built from *Duplex* steel to resist the transported chemicals, while the remaining structure is assumed to be of high tensile steel. *Duplex* steel yield strength is 440 MPa and that of high tensile steel is 355 MPa.

Tanker's structure is symmetric about the centre line. It is optimized through 47 longitudinal strakes of one half of the midship section. No fore- and aft-ship structure is considered, neither in analysis of hull response to normal service loads and collision loads.

The assumed section affected by collision includes the outer structure, starting 6310 mm from the centre line, i.e. the outer cargo tank, part of the double bottom and the whole double side as seen also in Fig. 5. Longitudinally, the section is bounded by two transverse bulkheads. For convenience, we name this section onwards as 'the crash section'.

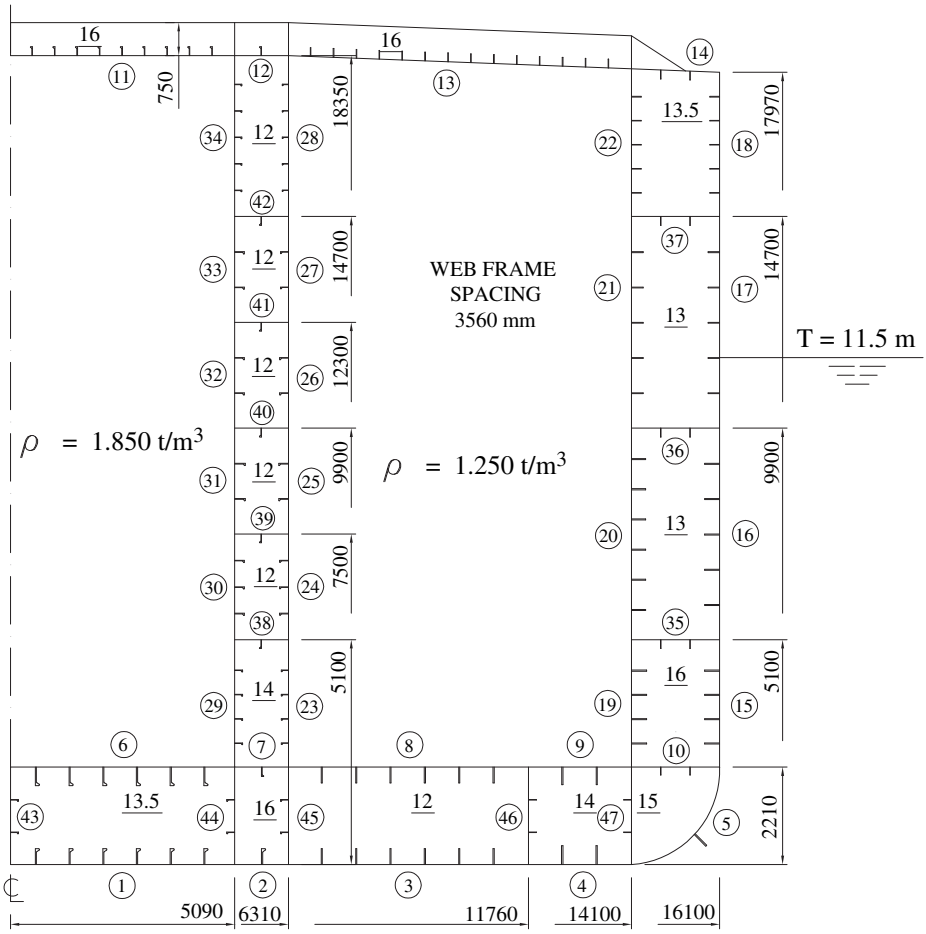

Fig. 4. Half of the main frame section of a considered tanker with dimensions in mm, indicated strake numbers (in circles) and scantlings of the transverse structures (underlined).

Each strake is generally described with five parameters: plate thickness, stiffener size, number of stiffeners, stiffener type and panel's material type. The former two parameters are varied in optimization, while the latter three are fixed. Their adopted values are seen also in Fig. 4. In total, the optimization is conducted with 94 variables.

Variables are considered discretely. The plate thicknesses are assumed to be available for every whole millimetre, from 5 to 24 mm outside the crash section, and in the crash section between 4 and 42 mm. The stiffener sizes are taken from the standard tables of profiles, e.g. Ref. [42], for the whole available range of HP profiles and flat bars. Flat bars are applied exclusively in the crash section only, due to their improved collision properties over HP profiles; see Ref. [10]. The flat bars undergo membrane stretching easier than HPs due to the reduced flexural stiffness. In other ship sections, HP profiles are used normally. Optimization of the transverse structures, i.e. the structure of the web frames, is not conducted, while its assumed scantlings are given in Fig. 4.

4.1.3. Constraints

Besides accidental loading, ship's structure needs to withstand normal service loads. We consider the hull girder loads and the lateral hydrostatic loads caused both by cargo and the sea. The effect of

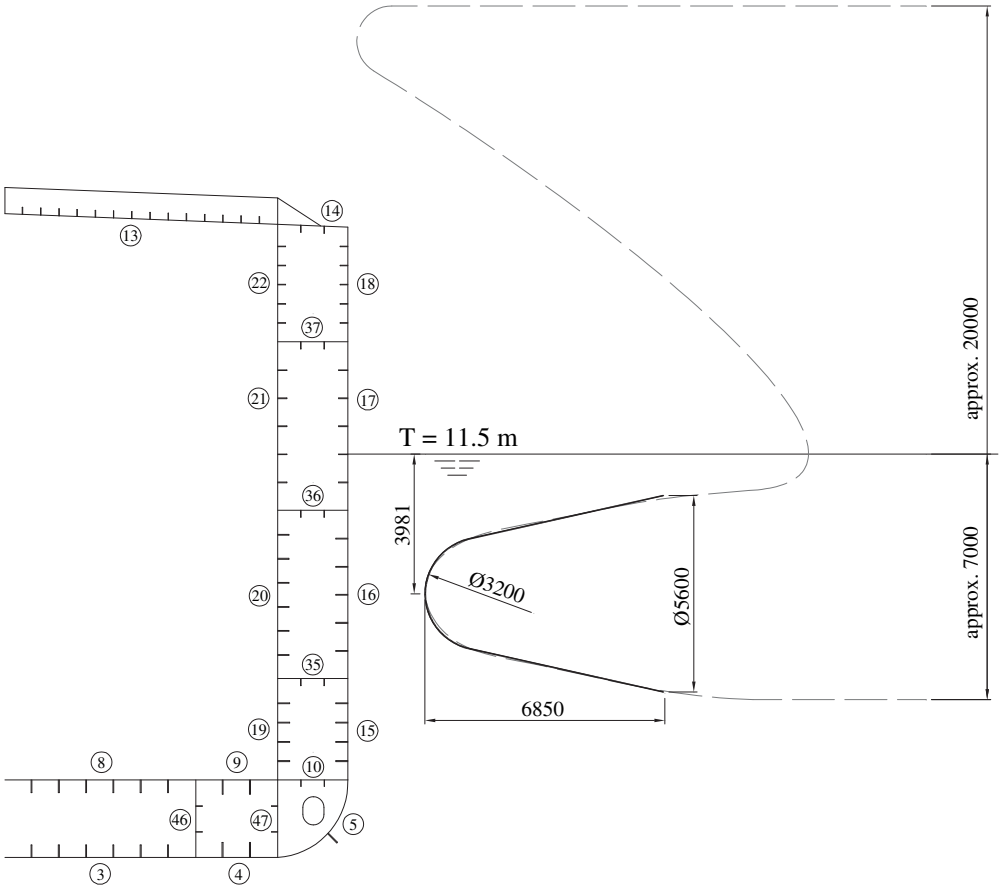

Fig. 5. Collision scenario (in realistic proportions) with indicated rigid bulb shape (bolded lines) used in FEM simulations and its accurate dimensions.

four critical hull girder loads is assessed at the two positions L/4 and L/2. For the former position, the shear force of 48 000 kN is applied both in hogging and in sagging, and for the latter, the total vertical bending moments of 2 932 000 kNm is applied in hogging and 2 452 000 kNm in sagging. The hydrostatic loads are specified based on the load height and on the density of the fluid ρ indicated in Fig. 4.

During the optimization the response under the hull girder loads is calculated applying the Coupled Beam (CB) method [43]. Local response of strake structures under hydrostatic loading is calculated with the uniformly loaded simple beam model, and it is added to the response of the structure to the hull girder loading. The structure of each strake is checked for eight standard failure criteria concerning: plate yield and buckling, stiffener yield, lateral and torsional buckling, stiffener's web and flange (where appropriate) buckling for each loading condition, see Ref [44] for more on their definition. Additional crossing over criterion [45] is used to ensure controlled panel collapse due to extensive in-plane loading. Altogether 376 failure criteria are calculated for each design alternative and for each loading condition. These criteria are confronted with the response through the adequacy functions, effectively describing optimization constraints. Adequacy is considered as a non-linear normalization function between the structural capacity of some structural element j, $a_j(\boldsymbol{x})$, and a loading demand acting on it, $b_j(\boldsymbol{x})$, as proposed in Ref. [14]:

$$g_j(\boldsymbol{x}) = \frac{a_j(\boldsymbol{x}) - |b_j(\boldsymbol{x})|}{a_j(\boldsymbol{x}) + |b_j(\boldsymbol{x})|} \tag{12}$$

This functions results with values ranging between −1 and 1. Zero delimits the feasible alternative with positive adequacy values from the infeasible, having a negative adequacy value.

4.2. Rapid numerical collision simulations

To evaluate crashworthiness during optimization, we need calculate it in significantly reduced time than commonly accepted, e.g. in the scale of 1 min. We therefore assume that collision occurs only with the bulbous bow, or the bulb, instead of the whole bow of a colliding ship (Fig. 5 depicts the assumed scenario). And that the bulb is rigid, so that only the tanker's structure absorbs the collision energy. Justifications for these simplifications are based firstly on the assumed bow shape, typical for the RoPax or a ferry of the considered size. In Fig. 5, it is possible to see that the remaining bow structure is unlikely, at full draughts of ships, to come into contact with the tanker before the bulb would penetrate deep enough and cause rupture of the inner hull. Secondly, ENERGY relates to the struck ship only and measures principally how much struck ship structure can tolerate collision energy before undergoing the breach.

LS-DYNA ver. 971 software package is utilized for numerical collision simulations. An FE model is created in ANSYS software based on the parametric input from the optimization algorithm. ANSYS performs pre-processing of the FE model, assigning element, nodal data and boundary conditions. LS-DYNA control parameters are automatically added in the batch call of LS-PREPOST software with a command file. After simulations, which yield forces on structure during collision, ENERGY is calculated through the force integration with the second batch call of LS-PREPOST.

4.2.1. FE model

FE model of the crash section is created for every alternative based on the predefined 3D geometry modelled in ANSYS software. An example is seen in Fig. 6. The FE model is constrained in the planes of transverse bulkheads to translate in all three directions. Following the recommendations of Refs. [23,46], the extent of such FE model is sufficient to avoid significant plastic deformations at its boundaries considering the size of the bulb and the extent of its penetration prior to inner hull breaching. Furthermore, preliminary simulation results yielded plastic strains on the boundaries at the magnitude of less than 10% of the maximum plastic strain obtained at the moment of hull breach.

Even though the geometry is re-meshed for every alternative, the following generic features are maintained. The size of elements for plating is established on the basis of stiffener spacing, being on average 0.8×0.9 m. To model the stiffeners, one element is used per stiffener height. This is a very coarse model, but bearing in mind that the ENERGY values are used only for comparison during the optimization, it can lead to a well represented structural response if it is combined with proper values of control parameters. The structure is modelled using strictly the four nodded, quadrilateral *Belytschko-Lin-Tsay* shell elements [47] with 5 integration points through their thickness.

4.2.2. Simulation control parameters

In comparison to the standard LS-DYNA hourglass control, *Flanagan-Belytschko* integration type control Refs. [46] is used, with an hourglass coefficient of 0.13205. This value was found iteratively for the considered coarse mesh to keep the hourglass energy in the single percents of the total energy.

The collision simulations are displacement controlled. The rigid indenter is moved into the structure with a constant velocity of 10 m/s. This velocity is found reasonable as it is still small enough not to cause inertia effects of the ship masses, see Ref. [25]. Ship motions are neglected and therefore not considered in the analysis.

The calculation time step is controlled based on the bar wave speed and the maximum of the shortest element side or the element area divided by the minimum of the longest side or the longest diagonal of the element. Instabilities for this time step could not be found. Additional mass scaling was not used to reduce the time step, due to the significant negative influence it possesses over the kinetic energy.

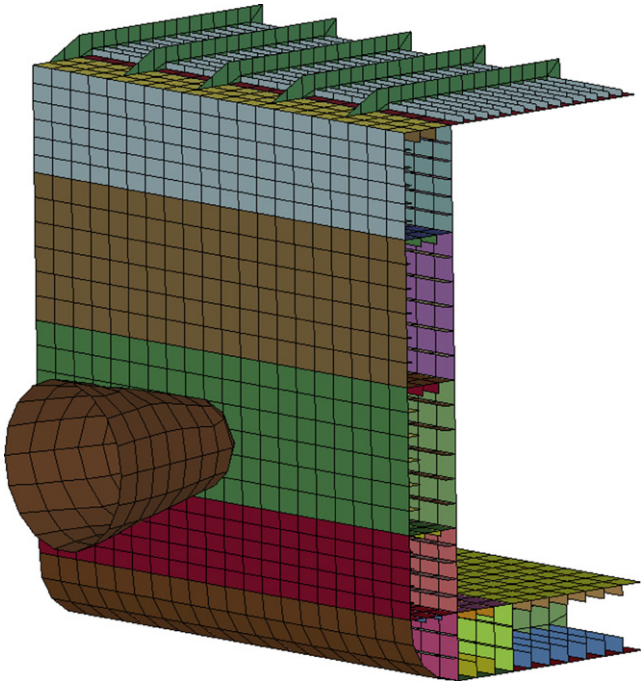

Fig. 6. Automatically generated FEM model for rapid assessment of crashworthiness of some design alternative.

*CONTACT_AUTOMATIC_SINGLE_SURFACE contact scheme of 'LS-DYNA' [47] is applied to treat the contact, where the reaction forces between structure and indenter are obtained by the *CONTACT_FORCE_TRANSDUCER_PENALTY card [47]. Additionally, only the minimal graphical output data is generated during the simulations to minimize hard disk activity during the simulation time. A static friction coefficient of 0.3 is used.

4.2.3. Material and fracture model

Material in the FE model is represented with the 'power law', where the strength coefficient K and the strain hardening index η are based on the tensile experiments [48]

$$\sigma = K \cdot e^{\eta}. \tag{13}$$

This material law is implemented to simulations as the Material 123 of 'LS-Dyna'. In the experiments, the K had a value of 730 for the standard steel with a yield stress of 284 MPa, but since we deal here with steel of higher strength than in the experiments K is scaled linearly. K then equals 1130 for the duplex steel and 912 for the high tensile steel. The strain hardening index $\eta = 0.2$ is assumed not to change, keeping the shape of the material behaviour in the simulations similar to that in the experiments.

The initiation and propagation of fracture is modelled by deleting the failed elements from the model. The *TERMINATION_DELETED_SHELLS_SET of LS-DYNA [47] was used to stop the simulation when the first element from the inner plate is removed, i.e. when the inner hull breaches. Fracture is addressed on the basis of computed strains. To evaluate the fracture-critical through thickness strain ε_f, we adopt the following empirical criterion [23,49]:

$$\varepsilon_f(l_e) = \varepsilon_g + \varepsilon_e \cdot \frac{t}{l_e} \tag{14}$$

where ε_g is the uniform strain and ε_e is the necking strain, t is the plate thickness and l_e is the individual element length. It is commonly recommended that the ratio l_e/t is not less than 5 for shell element. Respective uniform and necking strain values of 0.056 and 0.54 are obtained from the measurements of the plating damaged in collisions [48]. As shown in Ref. [50], this criterion is simple to implement into simulations, and more importantly it enables reasonable structural behaviour.

4.3. Optimization

4.3.1. The 'two-stage' optimization

The optimization is initiated with a population of 60 randomly generated design alternatives. This is considered sufficient, accounting for some preliminary results of the mass minimization for the same tanker, reported in Ref. [51]. The first stage minimizes HULL and DUPLEX without calculating ENERGY of the alternatives. Crossing over probability is $p_C = 0.8$, while mutation probability is $p_M = 0.0035$. Both values are set based on the previous experiences [18,52] and experimental runs. For the binary GAs, the standard mutation probability is determined as 1/(chromosome length), which in this case would be 0.0045. But since the variables are represented with short, four or five bit long, strings, a change in one bit, depending on the position, causes significant change in a variable that more probably degrades than improves the alternative's performance. Thus, the probability of mutation is reduced. The weighting factors for HULL and DUPLEX and all constraints, are equal to 2.646×10^{-3}, obtained from the fraction $l/(m+j)$, where m is taken as 2 and j equals to 376, since $w_{ENERGY} = 0$.

The minimization of HULL and DUPLEX is run until the 802nd generation as seen in Fig. 7a and b. At that point the rate of improvements decreases, and between the two objectives a small Pareto frontier is noticed. Assuming now that the further mass reductions will not be significant and that the 'light' alternatives have attained predominantly optimal variable values, the ENERGY maximization is added to the minimization of HULL and DUPLEX in order to generate the Pareto frontier between all three objectives. The second stage of the optimization is thus initiated. Fig. 7c–e depict this stage of optimization, where we see the rise in ENERGY. With the rise in ENERGY, the rise in HULL occurs as well, but every time VOP reaches some new ENERGY level, it follows up with the reduction in HULL. DUPLEX is not affected at all with the improvements in ENERGY until the very high levels of ENERGY are reached. After 350 generations the ENERGY starts to reach its upper limits.

Initially, the weighting factors in the second stage of optimization, including now the factor for ENERGY, are set to be equal to each other as in the first stage of optimization; see Table 1. In the first stage, ENERGY's weighting factor is zero, so the increase in its value leads VOP now to search the design space for alternatives with higher ENERGY. As it starts from one edge of the Pareto frontier, VOP generates additional Pareto optima while it maximizes ENERGY. This is assured by the fact that weighting factors of other objectives bear the same relative value as for ENERGY, but also due to the exploitation of the commonalities amongst Pareto optima which reduce the need for VOP to change many variable values. However, this search eventually stalls once the appropriate ENERGY level is reached for the applied weighting factors. This is seen to occur around 930th generation (Fig. 7e). Supposing that the equality between the weighting factors of the three objectives leads to the centre of the Pareto frontier, increasing ENERGY's factor beyond that of other objectives' 'pushes' the maximization of ENERGY further, eventually attaining the other edge of the Pareto frontier. However, the choice of the proper intensity for this increase relies on heuristic, following the basic argumentation of the previous sub-section. Therefore, additional adjustments in the weightings factors are made in the continuation of optimization until a desired progress is attained; see again Table 1 and Fig. 7. The second-stage is finalized once VOP fails to yield any new alternatives with higher ENERGY for the last 10 generations, in which HULL's and DUPLEX's weighting factors are set to zero. This then indicates that the edge of the Pareto frontier, where ENERGY attains its maximum, has been reached.

4.3.2. The results

In the end, VOP generates approx. 70 000 design alternatives, out of which 21 000 with the calculated ENERGY values. 1056 Pareto optimal alternatives are generated, ranging approx. over 2000t in HULL and 400t in DUPLEX. ENERGY is spread over 130 MJ. The Pareto front is fairly evenly developed between the objectives' extremes, allowing us to make relevant observations as seen in Fig. 8. Yet it is

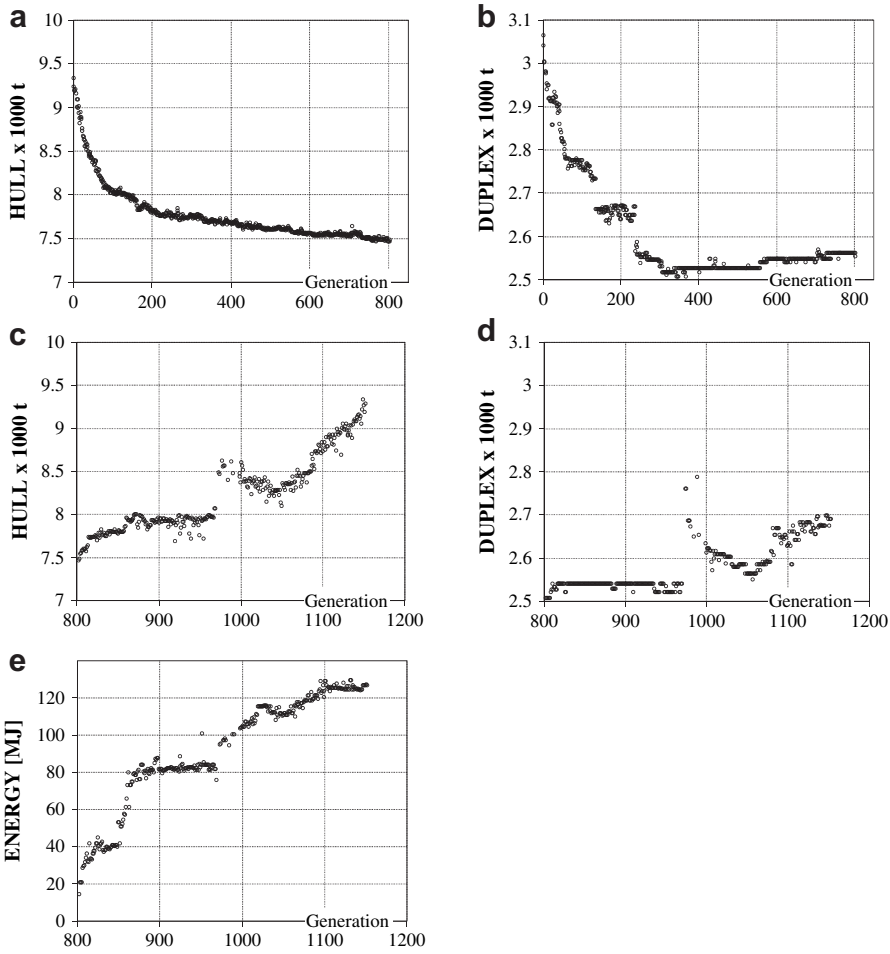

Fig. 7. Progress of optimization depicting best designs per generation for the particular objective, in the first stage, (a) and (b), and in the second stage, (c)–(e).

also rather extensive for the thorough analysis containing too many design alternatives. So due to the particular interest in maximizing ENERGY, and in seeing the effects it causes on the rise in masses, these 1056 relative Pareto optima are further filtered by simply maintaining several distinctive alternatives that are also Pareto optimal between the objective couples of ENERGY and HULL and ENERGY and DUPLEX. This filtered set contains now 32 alternatives indicated in Fig. 8.

From Fig. 8a and b we can now notice that the significant increase in ENERGY, from the lightest alternative with 10 MJ to the alternative with 90 MJ, is achieved practically without any increase in DUPLEX. Seemingly, only the outer shell is modified, but also mildly as seen also in Fig. 9. The increase in HULL, for a 'tenfold' increase in ENERGY, is only 25%. Furthermore, the amount of expensive *Duplex* steel can be kept at minimum for a fairly crashworthy design. This reduces the chance of unacceptable rise in costs for the increase in ship safety. Fig. 10 depicts the difference in scantlings for the two distinctive alternatives, 1 and 32, respectively being the HULL minimal and ENERGY maximal designs.

4.3.3. Validation of the rapid approach to assess crashworthiness

During the optimization, we applied the rapid approach to assess crashworthiness with a premise that it can yield sufficiently correct calculations of ENERGY to allow consistent comparison between the

Table 1
Heuristic of weighting factors w in the 'two-stage' optimization process (given values are relative).

Phase in omni-opt.	Generation		w_{ENERGY}	w_{HULL}	w_{DUPLEX}	w_{CONSTR}
	From	To	w_{CONSTR}	w_{CONSTR}	w_{CONSTR}	w_{CONSTR}
1	1	802	0	1	1	1
2	803	949	1	1	1	1
	949	959	3	1	1	1
	959	961	4	1	1	1
	961	975	5	1	1	1
	975	981	3	1	1	1
	981	991	2	1	1	1
	991	1010	2	0.5	0.5	1
	1010	1021	1.5	0.5	0.5	1
	1021	1037	1.5	1	1	1
	1037	1053	2	1	1	1
	1053	1060	3	1	1	1
	1060	1071	5	1	1	1
	1071	1138	5	0.5	0.5	1
	1138	1144	5	0.25	0.25	1
	1144	1153	5	0	0	1

generated alternatives. It fostered the coarse-meshed FE model. To validate this approach, a fine-meshed FE model is created now for each of the 32 Pareto optimal design alternatives, utilizing standard procedure for numerical collision simulations, similar to the procedure applied in Ref. [50]. ENERGY is recalculated for these models and obtained values are compared; see Fig. 11.

The average length of element in the fine-mesh model is reduced by three when compared to an element length in the coarse-mesh model. Therefore, there are at least three elements per stiffener height, and plates are meshed with elements of maximum size of 250×250 mm. This enables more accurate simulation of large structural deformations and of material fracture.

Observing now Fig. 11, it can be noticed that the fine-meshed model is less stiff, which leads to lower ENERGY values. This is of course expected since for the large ENERGY values, above 40 MJ, the structural deformations become large and the coarse-mesh model, due to its large finite elements, cannot sufficiently well capture the highly deformed shapes of the structure. However, the alternatives performing significantly better with the coarse-meshed model perform also better with the fine-meshed model.

Nevertheless, some inconsistencies can be noticed, predominantly for the small differences in ENERGY. To indicate the severity of these inconsistencies, two simple moving average curves in Fig. 11 are used. From their profile we find that a rise of at least 10 MJ of ENERGY in the coarse-meshed model probably results in a rise of ENERGY in the fine-meshed model. On the other hand, a rise of at least

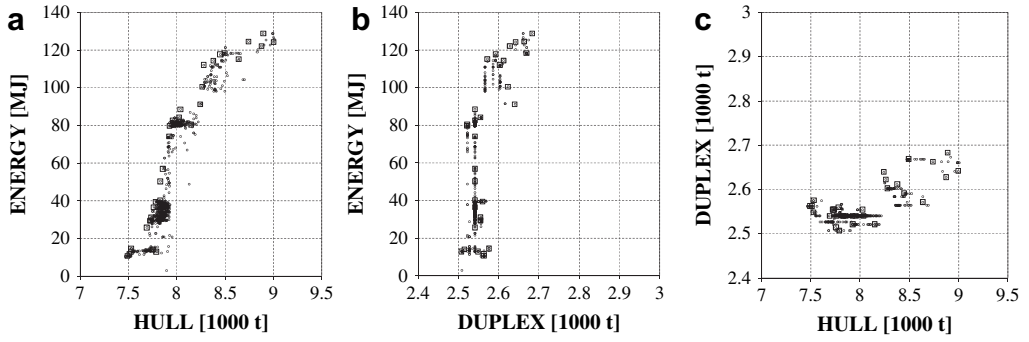

Fig. 8. Pareto optima (○) in the objective space, with 32 selected alternatives for further analysis (■).

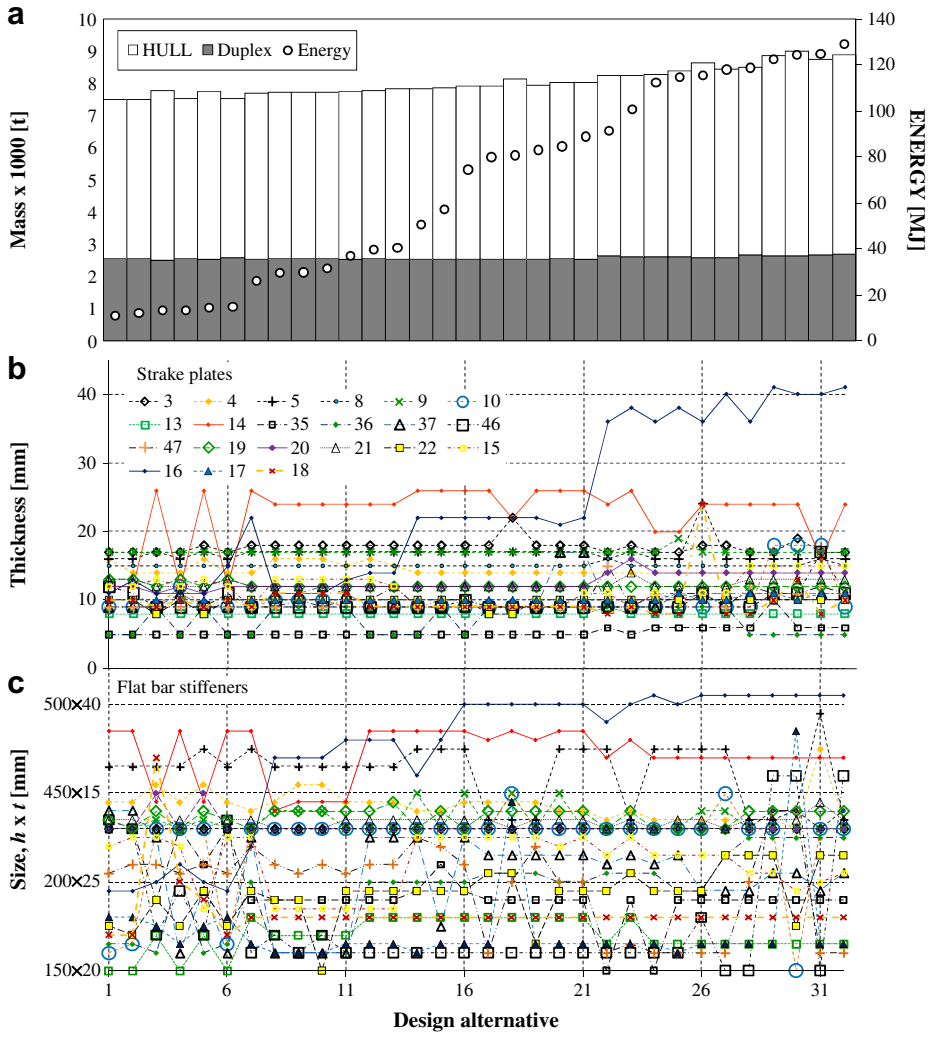

Fig. 9. Analysis of the 32 sorted Pareto optima according to the rising ENERGY: a) correspondence in rise between ENERGY, HULL and DUPLEX with b) plate thicknesses and c) stiffener sizes in the crash section.

20 MJ of ENERGY is certain to indicate rise in the fine-mesh model, accounting that this is valid solely for the considered example.

From this expose we can conclude that the error of the coarse-meshed model with respect to ENERGY is less than 20 MJ. Accounting that the optimization generated alternatives with the ENERGY spreading over 130 MJ, this error can be treated as acceptable, principally confirming the applicability of a coarse-mesh approach for relative comparison as required in optimization.

5. Discussion

The optimization of the case study yields a set of interesting findings, both about tanker crashworthiness and about optimization of crashworthy structures. These have potentially significant influence on design and therefore they are thoroughly discussed here.

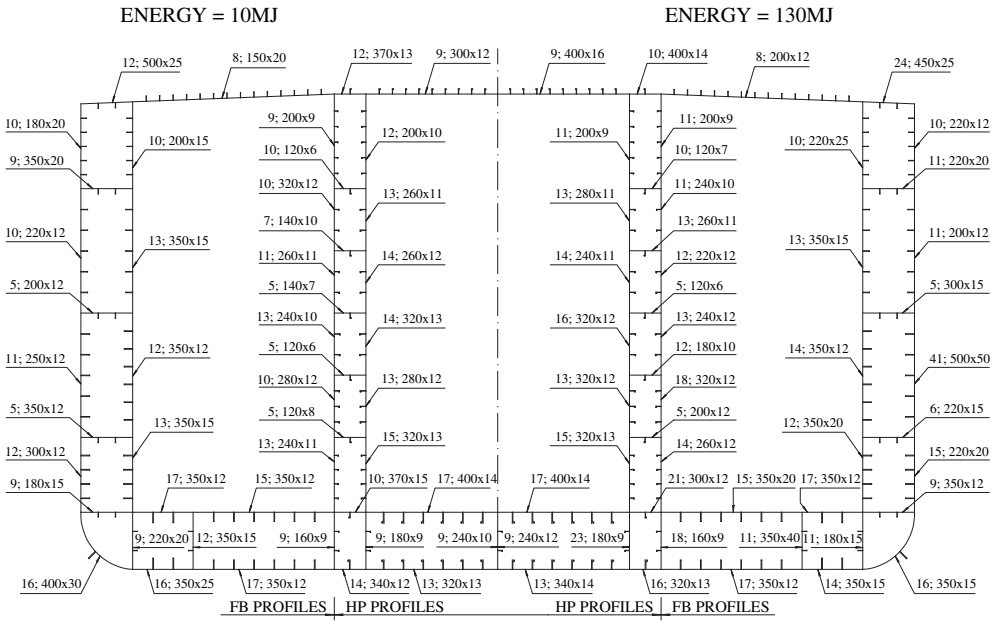

Fig. 10. Comparison of ENERGY for coarsely and finely meshed FE models for 32 Pareto optimal design alternatives with indicated 10 MJ and 20 MJ moving averages.

If we observe the rise in ENERGY in more detail, from the lightest to the heaviest design, we can easily notice where and when material is added to increase the crashworthiness of the structure. As seen from Fig. 9b and c, material addition is most intensive for the strake 16 in the outer shell, exactly where we expect the collision to occur, and in the strake 14. For the higher levels of ENERGY, above

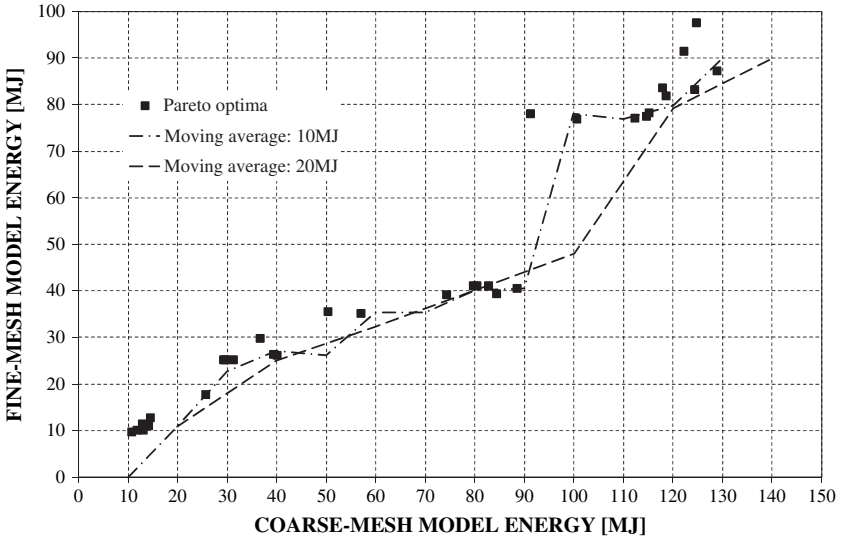

Fig. 11. Scantlings of the min HULL (10 MJ), on the left hand side, and max ENERGY (130 MJ) design alternatives (first number, before semicolon, represents the strake thickness, and the second represents the profile size).

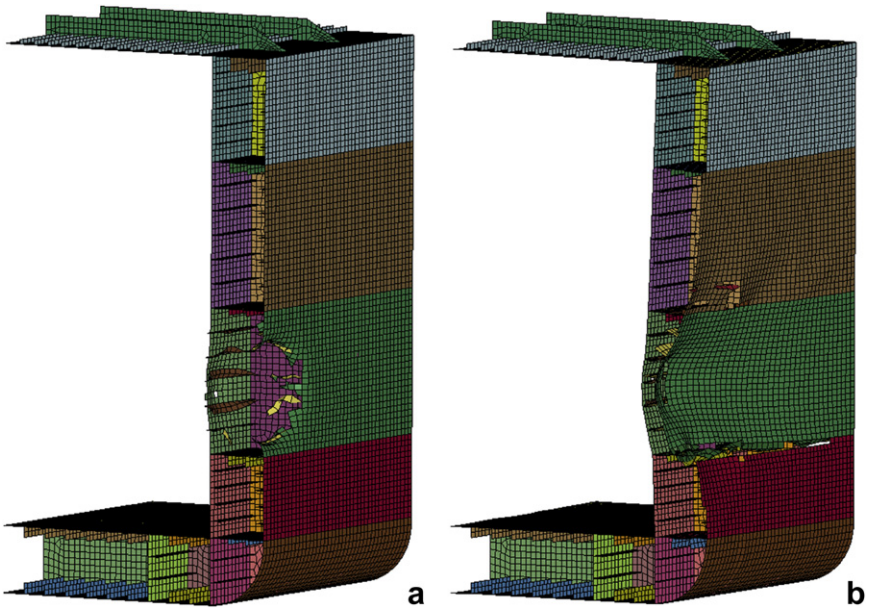

Fig. 12. Computed collision deformations, applying the fine-meshed FE model, for the a) min HULL/low crashworthy alternative 1, and b) max ENERGY/high crashworthy alternative 32, at the point of inner hull rupture.

100 MJ, material is slightly added to the inner shell, in strake 20, being directly behind the strake 16. Furthermore, if we compare Figs. 8 and 9, we can also see that for the fine-mesh calculations, ENERGY is strongly linked to the strake 16, where the major increases in ENERGY are analogous to the increases in the plating thickness and stiffener size of the strake 16; take also a special notice of the changes in ENERGY and plate thickness of the strake 16 between the design alternatives 21 and 22. On the other hand, the neighbouring side shell strakes, as well as the horizontal stakes of deck and double bottom, show no significant consistent changes, as indicated in Fig. 9. This leads to the conclusion that the increase in crashworthiness has been attained predominantly through the local stiffening, at the place of presumed collision.

This finding is physically justified with the observation of McDermott et al. [53] that most of the collision energy is absorbed by the membrane tension of the structural elements. So, if the structure is globally stiff, the initial collision deformations arising locally in the structure at the striking location will be constrained to dissipate and membrane tension will not develop sufficiently. This input of energy will raise plastic strains locally and eventually initiate fracture in the vicinity of the contact. If on the contrary a structure at the striking location is supported flexibly, but is locally stiff, the deformations will spread more easily, initiating membrane tension and dissipating the strains widely over the structure. For this reason their intensity will be low and fracture will be postponed. This can be clearly seen in Fig. 12 that depicts the calculated collision deformations at the moment of inner hull rupture for a low crashworthy (design alternative 1) and a highly crashworthy (design alternative 32) hull

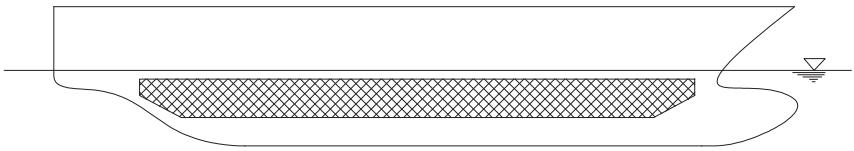

Fig. 13. Local strake stiffening extended over the whole length of the ship.

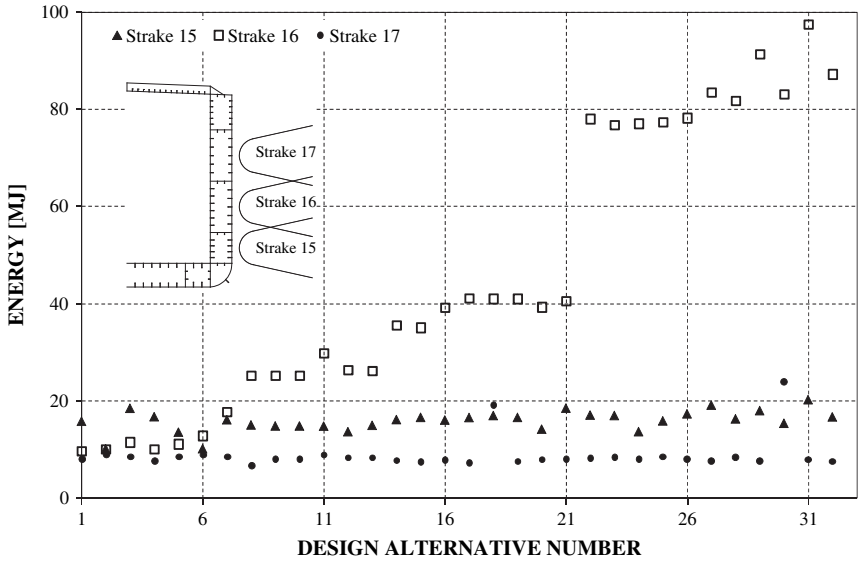

Fig. 14. Comparison of ENERGY values evaluated for the fine-meshed FE model at locations below (strake 15), on and above (strake 17) the locally stiffened strake 16 for the 32 Pareto optimal alternatives.

structure. The evidence of this reasoning can be found to exist in some other reported studies, including the results of the full scale collision tests [24], or in the numerical simulations analyzing these tests [25].

If we assume that serious and very serious collisions occur predominantly involve contact with bulbous bow, following this discussion we can suppose that an efficient mean to elevate crashworthiness is through the local stiffening that extends below ship's waterline. This proposal is symbolically depicted in Fig. 13, and it is similar to the better known 'ice belt', or more appropriately, to the 'torpedo belt' of the early 20th century naval ships [54]. Obviously, if the collision would occur above or below such a locally stiffened location, a significant difference in crashworthiness can be expected. To understand the extent of this difference, we perform additional collision simulations on the studied tanker assuming the same characteristics of the striking bulbous bow. The fine-mesh model is applied for the considered 32 Pareto optimal alternatives, and collision simulations are performed accordingly with striking positions on strakes 15 and 17, i.e. below and above the original struck strake 16. The results of these collision simulations are presented in Fig. 14, which shows that all simulated collisions on strakes 15 and 17 result in relatively similar values of ENERGY. Moreover, these ENERGY values do not reduce below the levels attained for the least crashworthy alternatives.

To end this discussion, we once again revert to the fact that optimization resulted with Pareto optimal alternatives that share most of the variable values. Knowing that commonality is the property related to the alternatives on a true Pareto frontier [38], we can conclude therefore that the attained alternatives are at least in its vicinity. More important, this outcome can be considered as the proof of applicability of the presented 'two-stage' optimization to solve practical problems. Furthermore, it serves as the proof of necessity to conduct optimization. The argumentation about the usefulness of local stiffening for crashworthiness is the direct outcome of optimization, and prior to optimization it was hardly conceivable as nothing similar was reported in the literature at best of our knowledge.

6. Conclusion

The objective of this paper was to study optimization of crashworthy marine structures. A 'two-stage' optimization procedure has been developed that allows practical execution of this objective. It

was illustrated on an example of tanker structure, where also a rapid approach to assess crashworthiness was introduced. In the end, the results of this study proved not only the capability of the introduced new approaches, but also indicated interesting new findings.

First finding is that the set of Pareto optimal alternatives between crashworthiness and hull mass have many common variable values. Since literature refers to the same observations for problems of smaller scale, this result is not a surprise, but it is an interesting fact, yielding two significant design benefits. The first is the clear separation of the variables to those that efficiently influence objectives, and which need to be changed to rationally improve design characteristics, and to those which affect the objectives negatively, and which should remain constant to guarantee rationality of a design alternative, i.e. its Pareto optimality. The second benefit is the enhancement of optimization due to a significantly reduced number of variables which need to be changed to construct a well developed Pareto frontier.

The second finding is the possibility to raise crashworthiness efficiently only by local stiffening in the area most critical for ship survivability – below the waterline. Specialty of this solution is that stiffening is local in vertical direction, i.e. it does not spread over the whole height of the ship.

Optimization of other crashworthy solutions should be also the topic of future research, e.g. optimization of the web frames, optimization of the enclosed structures, such as marketed *Y-core* structure. Efforts should be also made to understand the realistic benefits and sacrifices of raising crashworthiness. Safety and investments cannot be expressed in terms of megajoules of energy and tons of mass, nor can they be properly waged without understanding the industrial and societal needs for safety. In this paper, the optimization raised the crashworthiness of the tanker from the bottoms of 10 MJ needed to breach the hull to 130 MJ. But in reality what does this mean? Only the realistic setting would bring an answer to this question, one which fosters risk analysis and a formal assessment of industrial and societal preferences towards safety.

Acknowledgments

This study was supported by the IMPROVE project, funded by the *European Union* (Contract nr. 031382-FP6 2005 Transport-4), and the *Technology Development Centre of Finland – TEKES*, including Finnish shipbuilding industry, through the project *CONSTRUCT*. This help is here gratefully acknowledged.

References

[1] R. Italiana – Tribunale penale di Livorno Sez. 1 (R. Italy – Criminal court of Livorno Sec. 1). Sentence in a case against defendants of "Moby Prince" accident. Available at: http://www.mobyprince.it/files/Moby-Prince-Sentenza-1_(31.10.1998).pdf [accessed 4.08.08] (in Italian).
[2] International Maritime Organization. Casualty statistics and investigations: very serious and serious casualties for the year 1999. FSI.3/Circ.2, 2001; Available at: http://www.imo.org/includes/blastDataOnly.asp/data_id%3D5397/2.pdf [accessed 4.08.08].
[3] International Maritime Organization. Casualty statistics and investigations: very serious and serious casualties for the year 2000. FSI.3/Circ.3, 2002; Available at: http://www.imo.org/includes/blastDataOnly.asp/data_id%3D5118/3.pdf [accessed 4.08.08].
[4] International Maritime Organization. Casualty statistics and investigations: very serious and serious casualties for the year 2001. FSI.3/Circ.4, 2004; Available at: http://www.imo.org/includes/blastDataOnly.asp/data_id%3D8934/4.pdf [accessed 4.08.08].
[5] International Maritime Organization. Casualty statistics and investigations: very serious and serious casualties for the year 2002. FSI.3/Circ.5, 2005; Available at: http://www.imo.org/includes/blastDataOnly.asp/data_id%3D11539/5.pdf [accessed 4.08.08].
[6] International Maritime Organization. Casualty statistics and investigations: very serious and serious casualties for the year 2003. FSI.3/Circ.6, 2005; Available at: http://www.imo.org/includes/blastDataOnly.asp/data_id%3D11540/6.pdf [accessed 4.08.08].
[7] Wang G, Ji C, Kujala P, Lee S-Gab, Marino A, Sirkar J, Suzuki K, Pedersen PT, Vredeveldt AW, Yuriy V. Report of Committee V.1 Collision and Grounding. In: Proceedings of the 16th international ship offshore structures congress, vol. 2. UK; 2006. p. 1–61.
[8] Minorsky VU. An analysis of ship collision with reference to protection of nuclear powered plant. J Ship Res 1959;3(2):1–4.
[9] Simonsen BC. Ship grounding on rock—II. Validation and application. Mar Struct 1997;10(7):563–84.
[10] Alsos HS, Amdhal J. On the resistance to penetration of stiffened plates, Part I – experiments. Int J Impact Eng 2009;36(6):799–807.

[11] Klanac A, Ehlers S, Tabri K, Rudan S, Broekhuijsen J. Qualitative design assessment of crashworthy structures. In: Proceedings of the International Maritime Association of Mediterranean, Portugal. 2005. p. 461–9.
[12] Ehlers S, Klanac A, Tabri K. Increased safety of a tanker and a RO-PAX vessel by implementing a novel sandwich structure. In: Proceedings of the fourth international conference collision and grounding of ships. Germany: 2007. p. 109–15.
[13] Cho KN, Arai M, Basu R, Besse P, Birmingham R, Bohlmann B, Boonstra H, Chen YQ, Hampshire J, Hung CF, Leira B, Moore W, Yegorov G, Zanic V. Design principles and criteria. In: Proceedings of the 16th international ship and offshore structures congress. Southampton: 2006. p. 543–624.
[14] Hughes OF, Mistree F, Zanic V. A practical method for the rational design of ship structures. J Ship Res 1980;24(2):101–13.
[15] Rigo Ph, Fleury C. Scantlings optimization based on convex linearization and a dual approach – Part II. Mar Struct 2001;14: 631–49.
[16] Holland JH. Adaptation in natural and artificial systems. Ann Arbor: University of Michigan Press; 1975.
[17] Goldberg DE. Genetic algorithms in search, optimization and machine learning. Boston: Addison-Wesley Longman Publishing; 1989.
[18] Deb K. Multi-objective optimization using evolutionary algorithms. Chichester: John Wiley & Sons; 2001.
[19] Klanac A, Jelovica J. Vectorization in the structural optimization of a fast ferry. Brodogradnja-Shipbuilding 2007;58(l):11–7.
[20] Klanac A, Jelovica J. Vectorization and constraint grouping to enhance optimization of marine structures. Mar Struct 2009; 22(2):225–45.
[21] Deb K, Tiwari S. Omni-optimizer: a procedure for single and multi-objective optimization. In: Proceedings of the EMO 2005. Mexico: 2005. p. 47–61.
[22] Klanac A, Jelovica J. A concept of omni-optimization for ship structural design. Proc Adv Mar Struct, Scotland 2007:473–81.
[23] Zhang L, Egge ED, Bruhms H. Approval procedure concept for alternative arrangements. In: Proceedings of the third international conference collision and grounding of ships. Japan: 2004. p. 87–97.
[24] Wevers LJ, Vredeveldt AW. Full scale ship collision experiments 1998. Delft: TNO; 1999.
[25] Konter A, Broekhuijsen J, Vredeveldt A. A quantitative assessment of the factors contributing to the accuracy of ship collision predictions with the finite element method. In: Proceedings of the third international conference collision and grounding of ships. Japan: 2004. p. 17–26.
[26] Kitamura O. Comparative study on collision resistance of side structure. Mar Tech 1997;34(4):293–308.
[27] Sano A, Muragishi O, Yoshikawa T. Strength analysis of a new double hull structure for VLCC in collision. In: Proceedings of the international conference design and methodologies for collision and grounding protection of ships. USA: 1996.
[28] Kuroiwa, T. Numerical simulation of actual collision and grounding experiments. In: Proceedings of the international conference design and methodologies for collision and grounding protection of ships. USA: 1996.
[29] Paik JK, Pedersen PT. Modelling of the internal mechanics in ship collisions. Ocean Eng 1996;23(2):107–42.
[30] Paik JK, Thayamballi AK, Lee SK, Kang SJ. A semi-analytical method for the elastic–plastic large deflection analysis of welded steel or aluminium plating under combined in-plane and lateral pressure loads. Thin-walled Struct 2001;39(2): 125–52.
[31] Wierzbicki T, Abramowicz W. On the crushing mechanics of thin-walled structures. J Appl Mech (Trans ASME) 1983; 50(44):727–34.
[32] Abramowicz W. Crush resistance of 'T' 'Y' and 'X' sections. Technical Report 24-Joint MIT – Industry Program on Tanker Safety. Cambridge: MIT; 1994.
[33] Amdahl J. Technical note on the consequences of a floatel/platform collision. Trondheim: The Norwegian Institute of Science and Technology, Division of Marine Structures; 1982.
[34] Forsberg J, Nilsson L. Topology optimization in crashworthiness design. Struct Multidisciplinary Opt 2007;33(1):1–12.
[35] Pedersen CBW. Crashworthiness design of transient frame structures using topology optimization. Comput Meth Appl Mech Eng 2004;193(6–8):653–78.
[36] Pedersen CBW. Topology optimization for crashworthiness of frame structures. Int J Crashworthiness 2003;8(1):29–39.
[37] Redhe M, Forsberg J, Jansson T, Marklund P-O, Nilsson L. Using the response surface methodology and the D-optimality criterion in crashworthiness related problems: an analysis of the surface approximation error versus the number of function evaluations. Struct Multidisciplinary Opt 2002;24(3):185–94.
[38] Deb K, Srinivasan A. Innovization: innovating design principles thru optimization. In: Proceedings of the eighth annual conference genetic evolutionary computation. USA: 2006. p. 1629–36.
[39] Luetzen M. Ship collision damage. PhD thesis, Lyngby: Technical University of Denmark; 2001.
[40] Tuovinen J. Statistical analysis of ship collisions. M.Sc., thesis, Espoo: Helsinki University of Technology; 2005.
[41] Samuelides MS, Tabri K, Incecik A, Dimou D. Scenarios for the assessment of the collision behavior of ships. Int Shipbuilding Progr 2008;55:145–62.
[42] Ruukki. Hot rolled shipbuilding profiles. Available at: http://www.ruukki.com/www/materials.nsf/materials/6EBCE827F1708096C2257242004C0D65/$File/Shipbuilding_profiles_EN_0806.pdf?openElement [accessed 4.08.08].
[43] Naar H, Varsta P, Kujala P. A theory of coupled beams for strength assessment of passenger ships. Mar Struct 2004;17(8): 590–611.
[44] Det Norske Veritas. Rules for ships. Pt. 3 Ch. 1 Sec. 14 Buckling control. Hovik: Det Norske Veritas; 2000.
[45] Hughes OF, Ghosh B, Chen Y. Improved prediction of simultaneous local and overall buckling of stiffened panels. Thin-walled Struct 2004;42:827–56.
[46] Flanagan DP, Belytschko TA. Uniform hexahedron and quadrilateral with orthogonal hourglass control. Int J Numer Meths Eng 1981;17(5):679–706.
[47] Hallquist JO. LS-DYNA. Keyword user's manual, version 971. Livermore: Livermore Software Technology Corporation; 2007.
[48] Peschmann J, Kulzep A. Seitenkollision von Doppelhüllenschiffen (Side collision of double hull ships). AbschluBbericht zum Teil D2A. Hamburg: Hamburg University of Technology; 1999.
[49] Scharrer M, Zhang L, Egge E. Kollisionsberechnungen in schiffbaulichen Entwurfssystemen (Collision calculation in naval design systems). Bericht Nr. ESS 2002.183. Hamburg: Germanischer Lloyd; 2002.
[50] Ehlers S, Broekhuijsen J, Alsos HS, Biehl F, Tabri K. Simulating the collision response of ship side structures: a failure criteria benchmark study. Int Ship Progr 2008;55:127–44.

[51] Klanac A, Jelovica J, Niemelainen M, Domagallo S, Remes H, Romanoff J. Omni-optimization of a tanker. In: Proceedings COMPIT'08. Belgium: 2008. p. 537–51.
[52] Bäck T. Optimal mutation rates in genetic search. In: Proceedings of the fifth international conference genetic algorithms. USA: 1993. p. 2–8.
[53] McDermott JF, Kline RG, Jones Jr EL, Maniar NM, Chiang WP. Tanker structural analysis for minor collisions. SNAME Trans 1974;82:382–414.
[54] Attwood EL. War-ships. 3rd ed. London: Longmans, Green, and Co.; 1908.